High-field magnetic properties of the magnetic molecule $\{Cr_{10}Cu_2\}$

Larry Engelhardt
Department of Physics and Astronomy, Francis Marion University, Florence, South Carolina, 29501, USA

Catalin Martin, Ruslan Prozorov, and Marshall Luban
Department of Physics and Astronomy and Ames Laboratory, Iowa State University, Ames, Iowa 50011, USA

Grigore A. Timco and Richard E. P. Winpenny
School of Chemistry, The University of Manchester, Manchester M13 9PL, United Kingdom
(Received 17 September 2008; published 6 January 2009)

We present detailed magnetic measurements and the theoretical analysis of the recently synthesized magnetic molecule $\{Cr_{10}Cu_2\}$. Due to the heterometallic nature of this molecule, there are three distinct intramolecular interactions, which we describe using an isotropic Heisenberg model with three distinct exchange constants. The magnetic properties of the model are calculated using the quantum Monte Carlo method, including the low-field magnetic susceptibility $\chi(T)$ and the magnetization $M(H,T)$ versus magnetic field H up to the saturation field ($\approx$80 T) for arbitrary temperature T. Of particular relevance to experiment, we have calculated the full set of ground-state level-crossing fields corresponding to peaks in $\partial M/\partial H$ versus H for low T. A detailed search of the three-dimensional parameter space yields two well-separated sets of exchange constants, both of which give good agreement between the predictions of the model and the measured $\chi(T)$. The present low-temperature tunnel-diode resonator measurements provide values of ground-state level-crossing fields, as well as the level-crossing fields for certain low-lying excited states up to 16 T that are in good agreement with theory. The full set of theoretical crossing fields is very nearly equal for both sets of exchange constants. The theory also provides quantitative predictions for the site-dependent local magnetic moments of this molecule, which could perhaps be tested by future nuclear-magnetic-resonance measurements.

DOI: 10.1103/PhysRevB.79.014404 PACS number(s): 75.50.Xx, 75.10.Jm, 75.40.Mg, 75.40.Gb

I. INTRODUCTION

The field of molecular magnetism has developed rapidly since the early 1990s and the number of different species of magnetic molecules that have been synthesized is large and continues to increase rapidly.[1–4] Magnetic molecules are of great interest since they provide a very convenient platform for exploring fundamental issues in nanomagnetism. Of key importance is the fact that the magnetic interactions between molecules are generally ignorable as compared to intramolecular Heisenberg exchange interactions among a relatively small number of magnetic ions. A crystal sample can therefore be considered as a macroscopic ensemble of independent identical nanomagnets featuring a discrete spectrum of magnetic energy levels that originates from the intramolecular exchange interactions between the magnetic ions.

The magnetic molecule $\{Cr_{10}Cu_2\}$ has a cyclic hourglass shape.[5,6] Three distinct nearest-neighbor exchange interactions, shown schematically in Fig. 1, are introduced for describing this system, guided by the findings of detailed x-ray diffraction studies.[5] First, the ligands connecting neighboring Cr^{3+} ions (spin $s=3/2$) are the same (same bond lengths and bond angles) for each Cr-Cr pair. Therefore, each Cr-Cr bond is described by the same exchange constant, J_1, which is represented by thin lines in Fig. 1. Second, the ligands on opposite sides of a Cu^{2+} ion (spin $s=1/2$) are not the same so those bonds are described by two different exchange constants, J_2 and J_3, which are represented in Fig. 1 by thick lines and double lines, respectively. Finally, the molecule possesses 180° rotational symmetry so the Cr-Cu bonds on opposite sides of the molecule are described by the same exchange constant. Taking these symmetries into account leads to three different exchange constants.

The primary goal of the present work is to build a theoretical model based on the Heisenberg Hamiltonian—or equivalently, to determine exchange constants (J_1,J_2,J_3)—which will successfully describe magnetic measurements as both the temperature and the external magnetic field are varied. To accomplish this, we calculate the magnetic properties of the model using the quantum Monte Carlo method.[7] In Ref. 6, a detailed search of this three-dimensional parameter space—involving calculations for thousands of sets of exchange constants—revealed that there are two different sets of exchange constants that both provide agreement with the weak-field susceptibility $\chi(T)$ $[=M(H,T)/H$ for $H=0.1$ T$]$ that was measured using a superconducting quantum interference device (SQUID) magnetometer for temperatures ranging from $T=2$ to 300 K. In

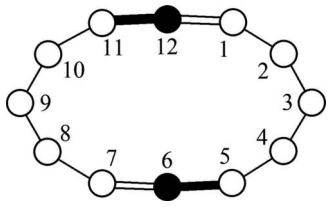

FIG. 1. The structure of the magnetic interactions for $\{Cr_{10}Cu_2\}$, where open circles represent Cr^{3+} ions and solid circles represent Cu^{2+} ions. The different line styles represent bonds with different exchange constants: J_1 (thin line), J_2 (thick line), and J_3 (double lines).

addition to the behavior of $\chi(T)$, we are also interested in the field dependence of the low-temperature differential susceptibility $\partial M/\partial H$ as these data can provide a direct experimental probe of the lowest-energy levels for different values of the total spin S. By contrast, the temperature dependence of χ provides a global probe of the complete energy spectrum, and a theory that successfully reproduces this quantity might not successfully describe the lowest-energy levels for different S. Data which address these questions are presented in Sec. II. In Sec. II A, we present theoretical predictions for the low-temperature differential susceptibility, which clearly show several peaks that correspond to ground-state level crossings occurring for $H<20$ T. The corresponding experimental measurements for H up to 16 T are shown in Sec. II B. We have used a tunnel-diode resonator (TDR) technique to obtain these data, and—as we show in Sec. II B and the Appendix—this method also provides information regarding field-induced crossings of excited-state levels. Both sets of level-crossing fields are in very good agreement with our theoretical model, as described in Sec. II C. Section III contains predictions of our theoretical model for future experiments regarding the magnetization for very high fields (up to 80 T) and the site dependence of the local magnetic-moment vector for the individual paramagnetic ions. Surprisingly, the same two sets of exchange constants, which equally well reproduce $\chi(T)$, also provide very similar quantitative results for the high-field magnetization and the local magnetic-moment vector. Finally, our results are summarized in Sec. IV.

II. MOLECULAR MAGNETISM

A. Theory

The magnetic structure of the $\{Cr_{10}Cu_2\}$ magnetic molecule was introduced in Sec. I, and using the notation of Fig. 1, we are adopting an isotropic Heisenberg Hamiltonian of the form

$$\mathcal{H} = J_1(\vec{s}_1\cdot\vec{s}_2+\vec{s}_2\cdot\vec{s}_3+\vec{s}_3\cdot\vec{s}_4+\vec{s}_4\cdot\vec{s}_5+\vec{s}_7\cdot\vec{s}_8+\vec{s}_8\cdot\vec{s}_9 + \vec{s}_9\cdot\vec{s}_{10}+\vec{s}_{10}\cdot\vec{s}_{11})+J_2(\vec{s}_5\cdot\vec{s}_6+\vec{s}_{11}\cdot\vec{s}_{12})+J_3(\vec{s}_6\cdot\vec{s}_7 + \vec{s}_{12}\cdot\vec{s}_1)+\mu_B\vec{H}\cdot\sum_{i=1}^{12} g_i\vec{s}_i, \quad (1)$$

where each spin operator $\vec{s}_i$ $(1\le i\le 12)$ is given in units of $\hbar$, μ_B is the Bohr magneton, and the numbering of the ions and the bonds are shown in Fig. 1. For the spectroscopic splitting factors, g_i, we use $g_i=1.98$ for the Cr^{3+} ions $(1\le i\le 5$ and $7\le i\le 11)$ and $g_i=2.10$ for the Cu^{2+} ions $(i=6$ and 12). The intrinsic spins are 3/2 for a Cr^{3+} ion and 1/2 for a Cu^{2+} ion. The total spin operators S^2 and S_z commute with $\mathcal{H}$ so the eigenstates of these operators are described by quantum numbers S and M_S whose values range from 0 to 16 $(=10\times 3/2+2\times 1/2)$ and from $-S$ to S, respectively.

This theoretical model involves a three-dimensional model parameter space (J_1,J_2,J_3); moreover, in Ref. 6, a detailed search of this parameter space revealed that there are two different sets of exchange constants that both provide excellent agreement with the measured weak-field susceptibility $\chi(T)$ for $H=0.1$ T and for temperatures ranging from $T=2$ to 300 K. These two sets of exchange constants will be referred to as model A, for which $J_1=14.8$ K, $J_2=52.9$ K, and $J_3=-11.8$ K; and model B, for which $J_1=16.9$ K, $J_2=27.2$ K, and $J_3=-13.1$ K. (Throughout this paper all energies, including the exchange constants, are given in units of the Boltzmann constant k_B.) The resulting data for $\chi(T)$, as obtained for both of these models, are shown in Fig. 2 along with the experimental data. Note that there are small deviations between these data below 10 K but when one examines the entire range of measured temperatures (from 2 to 300 K, shown in the inset of Fig. 2), the three data sets are nearly indistinguishable.

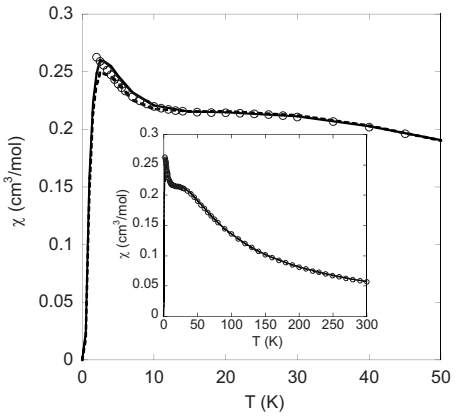

FIG. 2. Low-field magnetic susceptibility, $\chi=M/H$, versus temperature for $H=0.1$ T: Experiment (open circles), calculation for model A (solid line), and calculation for model B (dashed line). Values of the exchange constants for the two models are given in the text.

While this good agreement for $\chi(T)$ is essential for the development of a successful theoretical model, it is also necessary to test whether either or both of these models accurately predict the results of low-temperature field-dependent measurements since the latter data set can be used to provide detailed information concerning the values of the lowest-energy levels of Eq. (1) for each value of the total spin quantum number S. To that end, we have performed quantum Monte Carlo calculations of the low-temperature differential susceptibility $\partial M/\partial H$ for both of these theoretical models. These data are shown in Fig. 3 for $T=0.5$ K. The most striking feature of Fig. 3 is that the calculated results for the two models are very similar with only a slight deviation in the value of the field at which the third peak occurs. For both models, the first two peaks in $\partial M/\partial H$ both occur relatively close together $(H<5$ T), and the next peak does not occur until $H\approx 13$ T. Experiments have been performed to test these predictions, and these data are presented in Sec. II B.

B. Experiment

The real part, χ', of the dynamic magnetic susceptibility $(\chi=\chi'+i\chi'')$ of a $\{Cr_{10}Cu_2\}$ sample was measured using a TDR technique. The design and capabilities of a TDR are discussed at length elsewhere.[8,9] Briefly, steady-state oscillations with frequency $2\pi f_0=1/\sqrt{LC}$ are maintained in an

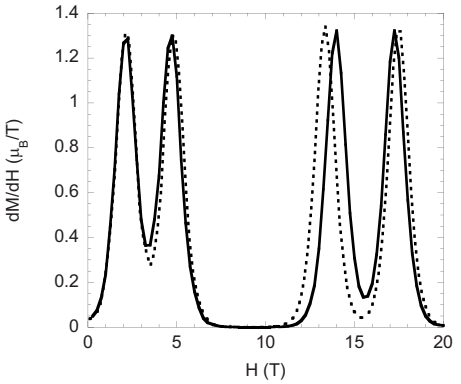

FIG. 3. Theoretical predictions for the differential susceptibility versus field for $T=0.5$ K. The solid line was calculated using model A, and the dotted line was calculated using model B (both described in the text).

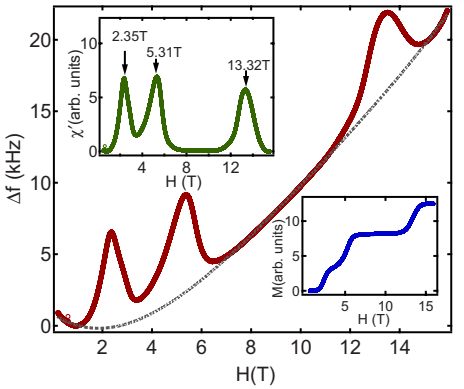

FIG. 4. (Color online) Main figure: Shift of the TDR frequency with applied magnetic field at $T=55$ mK with the sample inside the inductor (solid curve) and with an empty resonator (dashed curve). Upper inset: TDR signal after background subtraction, which is directly proportional to the real part χ' of the dynamic susceptibility. The field values for the peaks in χ' are indicated. Lower inset: Magnetization as obtained by integrating χ' (upper inset) with respect to H.

LC-tank circuit by a tunnel diode biased in its negative differential resistance region. When a sample is placed inside the inductor in the presence of a static field H, it produces a frequency shift Δf of the resonance frequency given by[10]

$$\frac{\Delta f}{f_0} \approx -\frac{1}{2}\frac{V_s}{V_c}4\pi\chi'(H,T,f_0), \tag{2}$$

where V_s and V_c are the volume of the sample and coil, respectively. A TDR operating at $f_0 \approx 15$ MHz with a stability better than 0.1 ppm was mounted on an Oxford dilution refrigerator Kelvinox400, equipped with a 14–16 T superconducting magnet. A special sample holder was designed to ensure good thermal coupling between the sample and the mixing chamber. The magnetic-field dependence of χ' was measured in isothermal conditions ($T \approx 50$ mK) by ramping up the magnetic field very slowly (0.01–0.03 T/min), ensuring thermal stability within 5 mK. There was no evidence of hysteresis effects as virtually identical results were obtained upon ramping down the magnetic field.

Figure 4 shows the change in the TDR frequency as a function of magnetic field at $T=55$ mK. Because of the magnetoresistance of the coil and some field dependence of the resonator capacitance, there is always a contribution from the empty resonator which appears as a background signal. To account for this, we have also measured the frequency shift in a separate run with an empty resonator. Then, by subtracting this background contribution, the field dependence of χ' is obtained up to a calibration constant. These data are shown in the upper inset of Fig. 4. For magnetic fields up to 16 T, three peaks in χ' were observed, occurring at $H=2.35$, 5.31, and 13.32 T. These peaks correspond to three steps in the magnetization M of the sample, shown in the lower inset of Fig. 4. This magnetization was calculated by integrating χ' with respect to H, which assumes $\chi' = \partial M/\partial H$ as described in the Appendix.

The effect of temperature on the peaks in χ' was further investigated by repeating our measurements for several higher temperatures, ranging from $T=55$ mK up to $T=3$ K, as shown in the inset of Fig. 5. When the temperature was increased from 55 to 100 mK, the results were virtually identical. However, as the temperature is increased further, new peaks began to emerge for $T \gtrsim 0.5$ K. These peaks are very prominent for $T=1.5$ K, as shown in Fig. 5. The values of the fields at which these new peaks occur are $H=3.94$ and 9.3 T, and their significance is discussed in Sec. II C.

C. Analysis

In Sec. II A, two sets of theoretical parameters were provided (models A and B), which give rise to the predicted field dependence of $\partial M/\partial H$ shown in Fig. 3 for $T=0.5$ K. Each of the peaks is associated with a ground-state level crossing, where the total spin quantum number S of the ground state changes by one unit. The level-crossing fields have also been measured experimentally (at $T=55$ mK, as shown in Fig. 4), and the predicted level-crossing fields for both models (A and B) agree very well with these low-temperature measurements. These data sets are summarized in Table I.

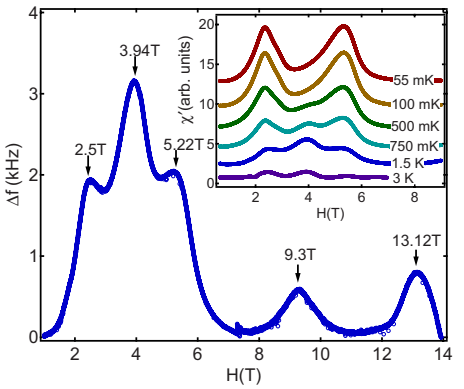

FIG. 5. (Color online) TDR signal after background subtraction at $T=1.5$ K. The field values for the observed peaks are indicated. Inset: TDR signal after background subtraction for several temperatures as marked on each trace.

TABLE I. Comparison between the predicted ground-state level-crossing fields for models A and B (from Fig. 3) and the corresponding measured level-crossing fields (from Fig. 4) for $T=55$ mK.

Model A (T)	Model B (T)	Experiment (T)
2.15	2.15	2.35
4.7	4.8	5.31
13.9	13.35	13.32

Based on the values of the three experimental level-crossing fields in Table I, one can infer the zero-field spacings of the lowest magnetic energy multiplets for this system for $S=0$, 1, 2, and 3. This is because each lowest-energy multiplet has $(2S+1)$-fold degeneracy when $H=0$; moreover, in an external magnetic field, the $(2S+1)$-fold degeneracy of each field-free multiplet is lifted due to a shift, $g\mu_B HM_S$, originating in the Zeeman term of Eq. (1). As the external field is increased from $H=0$, the ground state changes (among the members of these energy multiplets) successively from $S=0$, $M_S=0$ to $S=1$, $M_S=-1$, etc., in integer steps of S and M_S. Each of these changes of the ground-state quantum numbers is referred to as a level crossing, and the field at which the ground state changes from $S-1$ to S will be denoted H_S. Denoting the zero-field energy of the lowest-energy multiplets as E_S, the energy gap between these multiplets is given by $E_S-E_{S-1}=g\mu_B H_S$. Using this formula, the experimental data yield the energy-level diagram shown in Fig. 6, where each ground-state level crossing is indicated by a solid arrow, and level crossings involving low-energy excited states are indicated by open arrows.

In addition to the ground-state level crossings, several level crossings shown in Fig. 6 do not involve the ground state. These excited-state level crossings are not reflected in the (equilibrium) $\partial M/\partial H$ data shown in Fig. 3 but they *are* seen in our TDR measurements. This is because the TDR technique probes the dynamical susceptibility, which can reveal features that are not present in the static susceptibility.[11] As we describe in the Appendix, in order to observe these transitions between two excited states they must have a significant thermal occupation. This will occur if k_BT is comparable to the energy of the excited state, Δ (above the ground-state level for the given value of H). For the measurements shown in Fig. 4, the temperature was so low (55 mK) that the excited states have a negligible thermal occupation, and hence no transitions are observed between excited states. Although there are no excited-state level crossings that lie within milliKelvin of the ground state, there are three excited-state level crossings lying within $\Delta \lesssim 5$ K of the ground state, and these are indicated by open arrows in Fig. 6. In order to observe transitions associated with these level crossings, it is necessary to raise the temperature to $T \gtrsim 1$ K. These measurements were described in Sec. II B, and indeed peaks associated with these transitions are observed for $T=1.5$ K, as shown in Fig. 5.

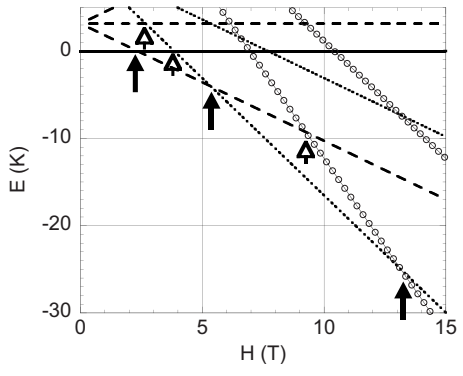

FIG. 6. Energy versus field for the lowest levels. These energy levels are inferred from the data in Fig. 4, and include states with quantum numbers $S=0$ (solid line), $S=1$ (dashed lines), $S=2$ (dotted lines), and $S=3$ (lines with circles). Solid arrows indicate ground-state level crossings, and open arrows indicate low-energy excited-state level crossings.

TABLE II. Comparison between predicted excited level-crossing fields and the fields associated with corresponding peaks in the measured TDR signal at $T=1.5$ K. (See the text for details.)

Predicted (T)	Measured (T)
2.7 ($\Delta \approx 3.6$ K)	2.5
3.85 ($\Delta \approx 2.0$ K)	3.94
9.25 ($\Delta \approx 5.2$ K)	9.3

The data associated with excited level crossings are summarized in Table II. Using the measured ground-state level-crossing fields that are listed in Table I, one directly obtains the predicted excited-state level-crossing fields. Those predictions are listed in the first column of Table II, along with the associated excitation energies, Δ. In the second column, we list the excited-state level-crossing fields as measured at $T=1.5$ K (from Fig. 5). Note that the first level-crossing field for $T=1.5$ K has a value of $H=2.5$ T, which is in between (and very close to) *two* level crossings: an $S=0 \rightarrow S=1$ (ground state) transition at $H=2.35$ T, and an $S=1 \rightarrow S=2$ (excited-state) transition at $H=2.7$ T. Given the close proximity (in H) of these level crossings, we believe it is likely that the ($T=1.5$ K) peak at $H=2.5$ T is a superposition of transitions associated with both of these level crossings. In addition to these transitions for which S changes by one unit, there are also peaks in the $T=1.5$ K data that correspond to $\Delta S=2$ transitions: The peak at $H=3.94$ T corresponds to an $S=0 \rightarrow S=2$ transition, and the peak at $H=9.3$ T corresponds to an $S=1 \rightarrow S=3$ transition. Although such $\Delta S=2$ transitions would *appear* to violate selection rules, these transitions are allowed if one adds a small contribution from non-Heisenberg terms to Eq. (1), as described in the Appendix. Taking this effect into account, the $T=1.5$ K data are in very good agreement with our model of the low-lying energy levels shown in Fig. 6.

In addition to being temperature dependent, the observation of peaks associated with excited-state level crossings also depends on the frequency f_0 of the measurement. As we describe in the Appendix, the Hamiltonian must include a

small contribution from non-Heisenberg terms which will cause a small energy gap (i.e., an avoided crossing) when two levels would otherwise cross. Furthermore, in order to observe these avoided level crossings, the frequency must satisfy the inequality $2\pi\hbar f_0 > \delta$, where δ is the energy gap associated with the avoided level crossing. Our TDR data were all measured at a single frequency, $f_0 \approx 15$ MHz, corresponding to an energy of $2\pi\hbar f_0 \approx 0.8$ mK. This implies that the energy gap δ associated with the avoided level crossings that we observe for excited states must satisfy $\delta < 0.8$ mK. As such, our observation of these excited-state level crossings places an upper limit on the size of these small energy gaps. If one were to lower the frequency, eventually these peaks should disappear for $2\pi\hbar f_0 < \delta$. The experimental verification of this prediction by future measurements would be useful for two reasons: First, it would provide additional support for our interpretation of the higher temperature (1.5 K) peaks in the TDR data. Second, this would demonstrate the effectiveness of the TDR technique as a method for measuring very small energy gaps associated with avoided level crossings of excited states. Finally, we remark that for ground-state level crossings (or avoided crossings) it is not clear whether or not the condition $2\pi\hbar f_0 > \delta$ is being met. This is because peaks arising from equilibrium fluctuations would still be observed at these level-crossing fields even for $f_0 = 0$ (static measurements). If the condition $2\pi\hbar f_0 > \delta$ *is* being met for the ground-state level crossings, one should observe a decrease in the amplitude of these peaks when f_0 is decreased so that $2\pi\hbar f_0 < \delta$ but modest peaks would still exist.

III. PREDICTIONS FOR FUTURE MEASUREMENTS

A. Ultrahigh-field magnetization

As we have shown in Sec. II, the theoretical predictions of both models A and B for the differential susceptibility of the $\{Cr_{10}Cu_2\}$ magnetic molecule are in very good agreement with our TDR data up to the highest measurable field (16 T). In addition, for both models we have calculated the magnetization M and differential susceptibility $\partial M/\partial H$ for higher fields up to the saturation field (≈ 80 T). Surprisingly both models continue to provide very similar results throughout this entire field range. In fact, these data are nearly indistinguishable when viewed on a scale that extends up to the saturation field so only the data for model A are shown here. These data (M and $\partial M/\partial H$ for model A) are shown in Figs. 7 and 8 for $T = 0.5$ K.

Examining Figs. 7 and 8, these predictions include several interesting features. As the field is increased from $H = 0$, there is a relatively wide plateau in $M(H)$ around 10 T, which has already been experimentally verified (in Sec. II). Then, as the field is increased further, $M(H)$ shows a series of many *roughly* equally spaced steps that occur between 14 and 50 T. The nature of these steps is clearly revealed by examining the corresponding $\partial M/\partial H$ data in Fig. 8. What appear as single rippled steps in M, with a change of approximately $4\mu_B$, are seen to correspond to closely spaced pairs of peaks in $\partial M/\partial H$. This can be seen by noting in Fig. 8 that $\partial M/\partial H > 0$ within these pairs while $\partial M/\partial H \approx 0$ between the pairs. This effect becomes consistently more pronounced as the field is increased to the point that two peaks nearly coincide at $H \approx 60$ T. Finally, the magnetization becomes saturated at $H \approx 80$, where one very large peak occurs, associated with a transition from an $S = 14$ ground state to an $S = 16$ ground state ("skipping" $S = 15$).[12] Several of the features predicted here could be tested at existing pulsed-field facilities for $H \lesssim 60$ T.

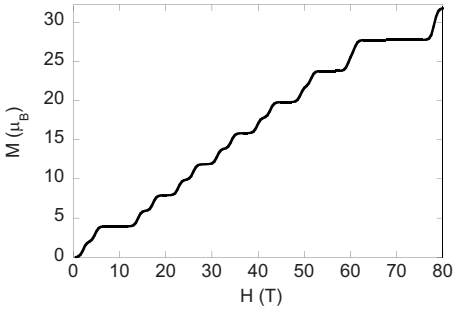

FIG. 7. Predicted M versus H for model A with $T = 0.5$ K, up to the saturation field (≈ 80 T).

B. Site dependence of the magnetism

In the course of our quantum Monte Carlo calculations, in addition to the magnetic properties of the molecule as a whole (M and $\partial M/\partial H$), we have also calculated the thermal equilibrium local magnetic moment of each of the 12 individual sites (paramagnetic ions) of the $\{Cr_{10}Cu_2\}$ magnetic molecule. Note that, for a (hypothetical) ring of N spins that is completely symmetric, this quantity would simply equal M/N for each site, and hence it would not be of interest. However, due to the relatively low symmetry of the present system (involving two different species of paramagnetic ions and three different bonds), the site-dependent magnetic moment has the potential to provide very rich data. This quantity has been calculated for a fixed low temperature ($T = 0.5$ K), and these data are shown in Fig. 9 for model A. (The corresponding data for model B are nearly indistinguishable from those of model A so only the data for model A are included.)

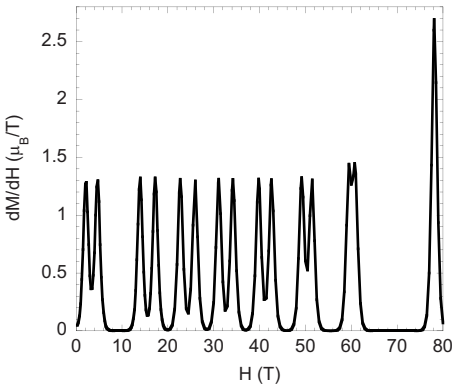

FIG. 8. Predicted $\partial M/\partial H$ versus H for model A with $T = 0.5$ K, up to the saturation field (≈ 80 T).

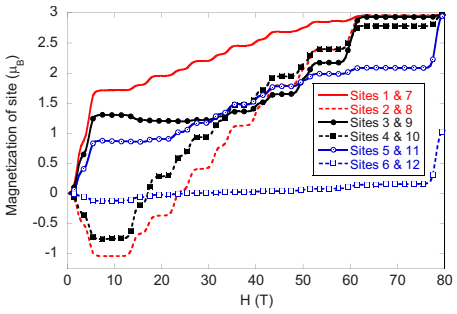

FIG. 9. (Color online) Predicted magnetic ordering of the equilibrium magnetic moment for the individual sites of the $\{Cr_{10}Cu_2\}$ molecule for $T=0.5$ K, up to the saturation field (≈ 80 T).

In order to interpret the predictions that are shown in Fig. 9, it is necessary to refer to the labeling convention that is defined in Fig. 1 and used in Eq. (1). Since the present system possesses 180° rotational symmetry, sites on opposite sides of the molecule are magnetically equivalent (e.g., site 1 is equivalent to site 7), and hence there are only six unique data sets to be shown in Fig. 9. Note that each of these six curves is quite distinct. As the field is increased from $H=0$ to $H\approx 5$ T, the local moments (specifically, the equilibrium local-moment vectors[13]) separate into those that point in the direction of the applied field (sites 1, 7, 3, 9, 5, and 11) and those that point in the opposite direction (sites 2, 8, 4, and 10) while the Cu^{2+} ions (sites 6 and 12) show almost no local moments until the saturation field is reached. This ordering persists from $H\approx 5$ to $H\approx 14$ T; then at higher fields, sites 2, 8, 4, and 10 "flip" in the direction of the applied field. (This occurs at $H\approx 15$ T for sites 2 and 8, and at $H\approx 25$ T for sites 4 and 10.) As the field is increased further, all of the local moments eventually reach their saturation value ($g_i s_i=2.97$ for the Cr^{3+} sites and $g_i s_i=1.05$ for the Cu^{2+} sites).

There are certain features of the local-moment data shown in Fig. 9 that are fairly intuitive to understand while other features would be quite difficult (probably impossible) to predict without these quantitative calculations. In particular, note that, in the vicinity of $H\approx 10$ T, the local moments become maximally staggered (with sites 2, 4, 8, and 10 reaching their most negative values). The value of the field at which this feature occurs could not have been predicted from a simple argument but the ordering of the sites is very easy to understand. It can be viewed in terms of a bipartite lattice of classical spin vectors, with one sublattice (composed of sites 1, 3, 5, 7, 9, and 11) pointing in the direction of the field and the other sublattice (sites 2, 4, 6, 8, 10, and 12) pointing in the opposite direction. Note that the Cu^{2+} ions (sites 6 and 12, for which $s=1/2$) reside on the sublattice that points in the direction opposite to the field, such that the net magnetization is positive. Although these two sublattices are easy to understand, the rankings of these local moments (e.g., site 1 > site 3 > site 5) could not have been predicted by simply inspecting the geometry of the molecule, and this therefore provides a nontrivial prediction for future measurements.

It would be very informative if the predicted behavior of the local magnetic moments could be tested by experiment.

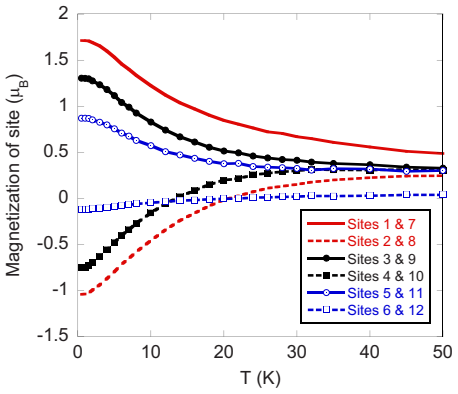

FIG. 10. (Color online) Predicted magnetic ordering of the equilibrium magnetic moment for the individual sites of the $\{Cr_{10}Cu_2\}$ molecule as a function of temperature for a fixed field, $H=10$ T.

This quantity has been successfully measured for different chromium-based magnetic molecule[14] using nuclear-magnetic-resonance (NMR) techniques. Specifically, the local moments of four nonequivalent Cr^{3+} sites in a Cr_7Cd magnetic molecule were observed by carefully studying the properties of an NMR spectrum. Such measurements are typically restricted to $H\lesssim 10$ T. We have therefore calculated the response of the individual local magnetic moments of $\{Cr_{10}Cu_2\}$ to a fixed field, $H=10$ T, and varying temperature, and the data are presented in Fig. 10. The local moments are roughly independent of temperature for $T\lesssim 2$ K. As the temperature is raised from $T=2$ to 10 K, the values of all of the local moments tend monotonically toward zero; and for $T>10$ K, the ordering of the local moments is lost. Therefore, temperatures in the range $T\lesssim 2$ K would be ideal for testing this phenomenon, and no ordering should be observable for $T>10$ K.

IV. SUMMARY

In this paper, we have provided several theoretical predictions for the magnetic behavior of the $\{Cr_{10}Cu_2\}$ magnetic molecule, as well as experimental measurements of certain relevant magnetic properties, and a detailed analysis of the relationship between the theoretical models and the experimental data. The theoretical predictions that have been presented are based upon two models (corresponding to two different sets of Heisenberg exchange constants), which we refer to as models A and B, both of which provide an excellent fit to the temperature dependence of the weak-field susceptibility $\chi(T)$, as described in Ref. 6. For both of these models, we have calculated the (predicted) low-temperature differential susceptibility $\partial M/\partial H$, which is presented in Sec. II A. These data are remarkably similar for both models, both exhibiting three nearly equal ground-state level crossings below $H=15$ T. These level-crossing fields have also been measured experimentally at a low temperature (55 mK) using a TDR technique (see Sec. II B), and the experimental results are in excellent agreement with the theoretical predictions. When the TDR measurement is repeated at a higher temperature (1.5 K), additional resonances are observed,

which are explained in terms of excited-state level crossings, as discussed in Sec. II C and the Appendix.

Notwithstanding the excellent agreement between experiment and the predictions of models A and B that are based solely on Heisenberg exchange, we cannot rule out the possibility that magnetic anisotropy terms might be of some significance for the present system. We note that our quantum Monte Carlo calculations have provided detailed field and temperature dependences of the differential susceptibility, and information concerning a relatively small subset of energy levels. If magnetic anisotropy plays a significant role, this will give rise to fine structure of the energy levels. A direct probe of the fine structure could be provided by high-frequency electron-paramagnetic-resonance measurements.[15]

In Sec. III, we have provided additional predictions that involve higher fields in the range of 16–80 T—which could be tested using pulsed magnetic-field techniques—and the site dependence of the local magnetic moments within a $\{Cr_{10}Cu_2\}$ molecule—which we hope can be tested using NMR techniques. In addition to achieving excellent agreement between theory and experiment, one of our most surprising findings is that both of the theoretical models (models A and B) provide virtually identical results for all of the magnetic properties that we have considered. As such, both of these models provide viable descriptions of the $\{Cr_{10}Cu_2\}$ magnetic molecule. We speculate that this virtual equivalence of distinct models is likely to be commonplace for spin models featuring the use of multiple exchange constants.

ACKNOWLEDGMENTS

We thank M. H. Lee for helpful discussions concerning linear-response theory. We also thank The Leverhulme Trust for supporting the collaboration between U.K. and U.S. groups. Work at the Ames Laboratory was supported by the Department of Energy—Basic Energy Sciences under Contract No. DE-AC02-07CH11358.

APPENDIX: DYNAMIC SUSCEPTIBILITY

In this Appendix we describe certain features of the dynamic magnetic susceptibility that provide a qualitative understanding of the TDR data of Sec. II B. For these measurements, the direction of the radio frequency magnetic field is collinear with the static magnetic field $\vec{H}$ so the dynamic susceptibility that is measured is the real part (χ') of the longitudinal component of the complex magnetic susceptibility $\chi_{zz}(\omega)=\chi'_{zz}(\omega)+i\chi''_{zz}(\omega)$.[10] From linear-response theory,[16] this quantity is given by

$$\chi_{zz}(\omega)=\chi_{zz}(0)\left[1-i\omega\lim_{\epsilon\to 0+}\int_0^\infty dt e^{-(i\omega+\epsilon)t}\times\left(\frac{\langle S_z(0)S_z(t)\rangle-\langle S_z\rangle^2}{\langle S_z^2\rangle-\langle S_z\rangle^2}\right)\right], \quad \text{(A1)}$$

where the angular brackets represent thermal averages, $S_z(t)$ is the Heisenberg representation (based on the system Hamiltonian $\mathcal{H}$) of the total spin operator S_z at time t, and $\chi_{zz}(0)$ is the static susceptibility. It is important to note that for nonzero values of ω the only nonvanishing contribution to $\chi_{zz}(\omega)$ originates exclusively from the time dependence of the quantity $\langle S_z(0)S_z(t)\rangle$. However, this thermal average is actually independent of time if the system Hamiltonian is restricted to being that for an isotropic Heisenberg model since the S_z operator commutes with $\mathcal{H}$. That is, $\chi_{zz}(\omega)$ is strictly zero for nonzero ω for this class of system Hamiltonians.

While the isotropic Heisenberg Hamiltonian of Eq. (1) provides an accurate model for static measurements of magnetization M and susceptibility $\chi_{zz}(0)$, it is subtly insufficient for determining $\chi_{zz}(\omega)$ for nonzero ω: the inclusion of very small non-Heisenberg terms that have been excluded from Eq. (1) is of vital importance. Their role is to allow for time-dependent contributions to

$$\langle S_z(0)S_z(t)\rangle=\frac{1}{Z}\sum_{\alpha,\beta}e^{-E_\alpha/k_BT}|\langle\alpha|S_z|\beta\rangle|^2e^{i(E_\beta-E_\alpha)t/\hbar}. \quad \text{(A2)}$$

Here $|\alpha\rangle$ and E_α, $|\beta\rangle$ and E_β denote eigenvectors and eigenenergies of $\mathcal{H}$. The key point is that numerous off-diagonal matrix elements $\langle\alpha|S_z|\beta\rangle$ that would vanish for a strictly isotropic Heisenberg model (hence yielding selection rules) are now nonzero and consequently $\langle S_z(0)S_z(t)\rangle$ becomes time dependent. However, for most applications, because of the smallness of the non-Heisenberg terms, it suffices to approximate the eigenenergies E_α by their unperturbed isotropic Heisenberg values.

These ideas can be further understood by considering the dynamical effects of a magnetic field being swept through a ground-state level-crossing field for a magnetic system at low temperatures. It is well known[17] that transitions between the two intersecting states would not occur if S^2 and S_z exactly commute with $\mathcal{H}$ [as is the case for Eq. (1)]; i.e., $M(H)$ would be constant for all H. That such transitions *are* observed experimentally as steps in $M(H)$ is a result of some (albeit small) contributions to $\mathcal{H}$ that does not commute with S^2 and S_z—e.g., spin-phonon coupling, etc. These small contributions to $\mathcal{H}$ cause small energy gaps (i.e., avoided crossings) to occur at what otherwise would be level-crossing fields, and they also cause the off-diagonal matrix elements in Eq. (A2) to be nonzero. Both of these effects are important to the following discussion.

Consider a general system Hamiltonian that does not exactly commute with S^2 and S_z. For this Hamiltonian, substituting Eq. (A2) into Eq. (A1) yields the result[18]

$$\chi'_{zz}(\omega)=\chi_{zz}(0)\left[1-\frac{\hbar\omega}{Z(\langle S_z^2\rangle-\langle S_z\rangle^2)}\times\sum_{\alpha,\beta}e^{-E_\alpha/k_BT}\frac{|\langle\alpha|S_z|\beta\rangle|^2}{\hbar\omega-(E_\beta-E_\alpha)}\right], \quad \text{(A3)}$$

which involves off-diagonal matrix elements $\langle\alpha|S_z|\beta\rangle$ that have a small but nonzero value, and a resonance occurs when $\hbar\omega=E_\beta-E_\alpha$. [This also provides contributions to $\chi''_{zz}(\omega)$ that are proportional to Dirac delta functions of $\hbar\omega-(E_\beta-E_\alpha)$.] The resonance condition will be satisfied in the vicinity of avoided crossings if $\hbar\omega\geq\delta$, where δ is the small energy gap

at the avoided crossing which results from the small non-Heisenberg terms in the Hamiltonian. Conversely, for $\hbar\omega < \delta$ no resonance occurs. Besides the requirement $\hbar\omega \geq \delta$, in order for $\chi'_{zz}(\omega)$ to be large in the vicinity of avoided crossings, the Boltzmann factor $e^{-(E_\alpha - E_g)/k_B T}$ cannot be too small (i.e., these resonances will not be observable if $k_B T \ll E_\alpha - E_g$), where E_g is the ground-state energy and $E_\alpha - E_g$ is the excitation energy. To summarize, peaks that are associated with excited-state (avoided) level crossings will be observable in the TDR data only if each of the following three conditions are met: (1) The off-diagonal matrix elements have a small but nonzero value due to non-Heisenberg terms. (2) The Boltzmann factors for these excited states are non-negligible, i.e., $k_B T \gtrsim E_\alpha - E_g$. (3) The frequency is sufficiently large compared with the energy gap at the avoided crossing, i.e., $\hbar\omega \geq \delta$.

[1] O. Kahn, *Molecular Magnetism* (VCH, Weinheim, 1993).

[2] D. Gatteschi, R. Sessoli, and J. Villain, *Molecular Nanomagnets* (Oxford Press, New York, 2006).

[3] R. E. P. Winpenny, J. Chem. Soc. Dalton Trans. **2002**, 1.

[4] R. E. P. Winpenny, Comp. Coord. Chem. II **7**, 125 (2004).

[5] M. Shanmugam, L. P. Engelhardt, F. K. Larsen, M. Luban, E. J. L. McInnes, C. A. Muryn, J. Overgaard, E. Rentschler, G. A. Timco, and R. E. P. Winpenny, Chem.-Eur. J. **12**, 8267 (2006).

[6] L. P. Engelhardt, C. A. Muryn, R. G. Pritchard, G. A. Timco, F. Tuna, and R. E. P. Winpenny, Angew. Chem., Int. Ed. **47**, 924 (2008).

[7] Matrix diagonalization methods are impractical for this system because the Hilbert space of the Hamiltonian matrix has dimension $D = 4^{10} \times 2^2 \approx 4.2 \times 10^6$. We instead use a quantum Monte Carlo method that was introduced in Ref. 19 and that has been used to successfully model other magnetic molecule systems (Refs. 6 and 20–25).

[8] C. T. VanDegrift, Rev. Sci. Instrum. **46**, 599 (1975).

[9] R. Prozorov, R. W. Giannetta, A. Carrington, and F. M. Araujo-Moreira, Phys. Rev. B **62**, 115 (2000).

[10] R. B. Clover and W. P. Wolf, Rev. Sci. Instrum. **41**, 617 (1970).

[11] M. D. Vannette, S. L. Bud'ko, P. C. Canfield, and R. Prozorov, J. Appl. Phys. **103**, 07D302 (2008).

[12] This type of anomalously large jump in M just below the saturation field is a general phenomenon for models of frustrated magnetic molecules (Refs. 26 and 27) and also occurs for models of large nonfrustrated homometallic antiferromagnetic rings (Ref. 22).

[13] This quantity is the canonical ensemble average of the quantum-mechanical (vector) spin operator associated with each individual magnetic moment.

[14] E. Micotti, Y. Furukawa, K. Kumagai, S. Carretta, A. Lascialfari, F. Borsa, G. A. Timco, and R. E. P. Winpenny, Phys. Rev. Lett. **97**, 267204 (2006).

[15] D. Zipse, J. M. North, N. S. Dalal, S. Hill, and R. S. Edwards, Phys. Rev. B **68**, 184408 (2003).

[16] R. Kubo, J. Phys. Soc. Jpn. **12**, 570 (1957), especially Eq. 3.5.

[17] A brief review is given in S. Miyashita, K. Saito, H. Kobayashi, and H. de Raedt, RIKEN Rev. **27**, 57 (2000).

[18] For a single species of magnetic ions, $\chi_{zz}(0)$ and $\langle S_z^2 \rangle - \langle S_z \rangle^2$ differ by a simple multiplicative factor. However, for the two-species system of our present study, where the spectroscopic factors of the Cr and Cu ions differ, the general form of Eq. (A3) applies.

[19] O. F. Syljuåsen and A. W. Sandvik, Phys. Rev. E **66**, 046701 (2002).

[20] G. J. T. Cooper, G. N. Newton, P. Kögerler, D.-L. Long, L. Engelhardt, M. Luban, and L. Cronin, Angew. Chem., Int. Ed. **46**, 1340 (2007).

[21] S. T. Ochsenbein, F. Tuna, M. Rancan, R. S. G. Davies, C. A. Muryn, O. Waldmann, R. Bircher, A. Sieber, G. Carver, H. Mutka, F. Fernandez-Alonso, A. Podlesnyak, L. P. Engelhardt, G. A. Timco, H. U. Güdel, and R. E. P. Winpenny, Chem.-Eur. J. **14**, 5144 (2008).

[22] L. Engelhardt and M. Luban, Phys. Rev. B **73**, 054430 (2006).

[23] A. M. Todea, A. Merca, H. Bögge, J. van Slageren, M. Dressel, L. Engelhardt, M. Luban, T. Glaser, M. Henry, and A. Müller, Angew. Chem., Int. Ed. **46**, 6106 (2007).

[24] A. Müller, A. Todea, J. van Slageren, M. Dressel, H. Bögge, M. Schmidtmann, M. Luban, L. Engelhardt, and M. Rusu, Angew. Chem., Int. Ed. **44**, 3857 (2005).

[25] L. Engelhardt, M. Luban, and C. Schröder, Phys. Rev. B **74**, 054413 (2006).

[26] J. Richter, J. Schulenburg, A. Honecker, J. Schnack, and H.-J. Schmidt, J. Phys.: Condens. Matter **16**, S779 (2004).

[27] J. Schulenburg, A. Honecker, J. Schnack, J. Richter, and H.-J. Schmidt, Phys. Rev. Lett. **88**, 167207 (2002).